

# Photonic classification on a single diffractive layer

Anil J. Pekgöz,<sup>1,2,\*</sup> Emre Yüce,<sup>1,\*</sup>

<sup>1</sup> Programmable Photonics Group, Department of Physics, Middle East Technical University,  
06800 Ankara, Turkey

<sup>2</sup> Quantum Science and Technology M.Sc., School of Natural Science,  
Technische Universität München, 85748 Garching, Germany

\*Corresponding Author: eyuce@metu.edu.tr  
anil.pekgoez@tum.de

**Photonic computation started to shape the future of fast, efficient and accessible computation. The advantages brought by light based Diffractive Deep Neural Networks (D2NN), are shown to be overwhelmingly advantageous especially in targeting classification problems. However, cost and complexity of multi-layer systems are the main challenges that reduce the deployment of this technology. In this study, we develop a simple yet extremely efficient way to achieve optical classification using a single diffractive optical layer. A spatial light modulator is used not only to emulate the classifying system but also the input medium for the objects to be classified by the system. Using our approach, we classify road traffic signs which has a direct application on daily life and safety. We perform classification of road signs under the effect of noise and show that we can successfully classify road signs with more than 75% accuracy under 20% noise/imperfection.**

## Introduction

The advantages of Artificial Intelligence (AI) gained extra ordinary levels in our today's world. From real time image recognition to cognitive copilots have showed us the potential of AI systems and the need of further development. However, the efficiency aspect of the newly system is as important as further developing the capabilities of new generation AI systems.

The imposed heavy computation and low parallelizability [1] (layer by layer computation) of Deep Neural Networks (DNN) on silicon-based processors creates the problem of significant energy consumption [2] and long process time arises the challenge of seeking alternative basis for Neural Networks. One of those alternative is the Diffractive Deep Neural Network (D<sup>2</sup>NN) which basis on the light diffraction theory [3] to emulate the Neural Network. The advantages of D<sup>2</sup>NN systems are: power efficiency [4] and the incredible speeds [5] relative to the common Deep Neural Networks which are based on silicon processors.

Pioneering studies have shown that it is possible to design a system [6] which is based only on Spatial Light Modulators (SLM) to simulate neurons and their interconnections to classify Modified National Institute of Standards and Technology database (MNIST database) numbers [7] and fashion objects [8]. Moreover, another research [9] has shown that numbers can be classified with only a Digital Micromirror Device, as the input layer, and a SLM, as the classifying layer, where the input layer is used to feed the information onto the SLM which classify it adaptively. The potential of easy applicability of D<sup>2</sup>NN systems have been proven [10] in a system of 3D printed Diffractive Optical Elements (DOE) where each DOE layer acts as a neural layer. Another applicability example [11] is using Electromagnetic Waves at the radio wave frequency range as a basis for a D<sup>2</sup>NN to perform various classification tasks.

However, the multi-layer D<sup>2</sup>NN systems [6, 9, 10, 11] proposes the problem of being layer-wise

complex in structure. This complexity limits the fields of application where low design time and cost-effectiveness is the main objective. Moreover, the correlation of training time and overall network complexity also imposes a challenge throughout the project. Therefore, it is hard to scale-up the layer structure since it can potentially increase the training duration [12].

With this challenges in mind, we are proposing a true single layer optical classifier where the input and classifier layer are combined in a single diffractive layer. In the proposed system, the single diffractive layer is simulated via an SLM. Since the input and classifier layer are combined on the same plane, the theoretical and methodological approach simplified substantially and proves both the possibility of optical classification without the deep layers and using just one single layer. The system's optimization algorithm is mostly based on the Gerchberg-Saxton algorithm [13, 14] with a basic spatial restriction. The performance of our system archives diagonality of test and prediction histograms and confusion matrices. Moreover, the performance of our method is not deteriorated in the presence of noise unlike the Neural Networks that are intolerant to noise [15, 16].

## Results and Discussion

The system which is used to classify the objects is based on the system given in Fig 1A. The light source is a semiconductor diode laser with a wavelength of 632 nm where the output beam is corrected with an array of ND filters for a suitable lasing power. The width of the beam is widened with a Gaussian Beam Expander such that the beam covers the SLM's surface. The Polarized Beam Splitter (PBS) acts both as a redirector of the reflected beam from the SLM and also as a polarizer which aligns the polarization of the laser beam to the SLM's polarization angle. The modulated beam is then redirected to the 4F system where only a small region of the frequency space is let through to eliminate the high intensity central point which is created as a side product from the modulation process, shown as in Fig 1B. The filtered laser beam is then redirected with multiple mirrors into the last lens in front of the camera which performs a Fourier transformation [3] from the spatial domain to the frequency domain.

The surface of the SLM is spatially divided into sub-surfaces according to the number of objects. This approach is used to optimize each object individually to its respective sub-surface. Since the sub-surfaces are spatially divided, the sub-surfaces are not interacting with each other on the surface level on the SLM. The binary shape of the object is written onto those sub-surfaces to establish the spatial restriction on the Gerchberg-Saxton Algorithm. To increase the used space on each sub-surface, the binary image of the object is written in a multiple-grid shape onto the sub-surface. The combined area which is going to be used in optimization process is named as Classifying Pixels. The area which is outside Constructive Pixels is used to diverge the light power outside the target and is named as Discriminating Pixels. This process of dividing the surface of the SLM and writing the binary object as grid-wise manner is shown in Fig 2. Given the circular nature of the Laser Beam in our case, the center 600 pixels to 600 pixels square region is actively used in this process.

The spatial restriction which has been defined in Fig 2. is used as the spatial restriction at the Image Plane [14] in the Gerchberg-Saxton Algorithm in each iteration. This spatial restriction is used as the modifiable areas for phase optimization on the SLM and can be also called as a restricted phase mask since the phase optimization is only done on a specific area. The area is defined as the binarized form [17] of the used dataset of 9 standard traffic signs. The mathematical representation of the process is as follows:

$$\Psi_{0,i}(x, y) = A_0(x, y) \exp(i\phi'_{0,i}(x, y))$$

Where  $\Psi_{0,i}$  is the subwavefront of 0-th iteration of the i-th object from the restricted SLM space and  $A(x, y)$  is the amplitude distribution of the laser's wavefront. The  $\phi'_{0,i}(x, y)$  is the restricted phase mask, which is defined as:

$$\phi'_{0,i}(x, y) = B_i(x, y) \odot \phi_{0,i}(x, y)$$

The  $B_i(x, y)$  is the binary form of the Spatial Restriction Array and  $\phi_{0,i}(x, y)$  is the initial phase mask, which is generated randomly initially. This part is depicted visually in Fig 3. The  $B_i(x, y)$  is divided in a 4 by 4 grid with the i-th object for efficient space usage. With 9 objects, the SLM is divide in 12 by 12 grids in total. This results in a 200 pixels by 200 pixels of Spatial Restriction Array with 50 pixels by 50 pixels of single image resolution.

The optimization of each sub-surface's phase mask,  $\phi'_{0,i}(x, y)$ , have been done with 20 iteration of the Spatially Restrictive Gerchberg-Saxton algorithm. This results in a total of 200 iteration including the Discriminating Pixels surface. The total duration of optimization took 20 minutes with a single core (Intel i7-10750H) and since the sub-surfaces are independent from each other, the duration could be shortened to almost 4.8 minutes with 6 parallel cores and a paralellity fraction of  $p \approx 0.95$  according to Amdahl's Law in our case [18, 19].

The initial test on the resulting phase plate generated via the described process in Methods Section is the power distribution test with the initial images to evaluate the performance on perfect conditions. With this aim, every initial object have been grided as 12 by 12 to cover the surface of our SLM. The normalized histogram results are shown in Fig 4A. The diagonallity shows us that the phase plate is focusing most of the laser power onto the wanted targets. On Fig 4B, the gray-scale camera images with false colormap and with their target boxes are shown. From the histogram in Fig 4A, it is clearly visible that the focused energy mostly hits on the designated target with some noise on other targets. Therefore, using the target with the most energy focused on, it is possible to correlate the input and the predicted label easily.

To test the validation performance with different levels of noise, 20 datasets have been generated where each dataset have a predefined percentage of random noise. Each dataset has 9,000 images which are equally distributed among 9 objects. The noise percentage ranges from 1% to 20% with a step size of 1%. The target with the most power concentrated is used to determine the predicted object in the testing phase. Three resulting confusion matrices for 1%, 5% and 10% and corresponding samples are shown in Fig 5A. With this algorithm, we managed to reach to a validation percentage of 96.26% for 10% noise. The total validation percentage for each dataset representing different noise level is shown in Fig 5B. We can archive a validation rate more then 90% till 13% noise level. Moreover, since the size of each dataset is equal, we can also calculate the combined validation average of 20 datasets. This average validation performance of 180,000 images with various noise levels equals to 91.78%.

The single layer nature of our proposed system showed us the possibility of optical classification via an novel method which is not directly connected to the fundamental working principles of interconnected neurons which spans over multiple layers like in DNN systems [20] and a D<sup>2</sup>NN systems. It is important to state that this new approach could be also adopted to the silicon based

computation.

In our experimental setup, we used the Holoeye LC-R 720 as our SLM. The phase shift capability in the specific configuration is  $1.81\pi$ . This fact causes an inefficient wavefront shaping since the whole phase range of  $2\pi$  was not available [14, p. 186]. Therefore, with a better phase shift range, higher validation percentages could be reached. Moreover, the repetition of the images in a grid-wise manner acts as a grating which produces unintentionally an interference pattern which overlaps the target areas. This interference pattern could be removed via studying the pattern behavior to modify the Discriminating Pixels such that it interferes destructively with the patterns in question.

The one-to-one linear scaling of the Image Plane and the Fourier Plane causes a significant problem on low resolution work space on a SLM. This problem is the precision and resolution of the generated target areas since it is bounded on the Image Plane's size and resolution. A smaller target size increases the validation efficiency and could also be scaled up with an optical magnifier system. However, the limit of the target size is bounded on the lowest achievable pixel size in the optimization algorithm which is also bounded by the SLM.

This method is a simple yet novel way to classify objects. The nature of not using any deep layers proposes a new elementary approach which can simplify system structure. Moreover, the system can be also further improved with an end classifier to get better noise vs validation performance results.

# Methods and Materials

## **Spatially Restrictive Gerchberg-Saxton Algorithm**

In the classification process, a Gerchberg-Saxton Algorithm is used to optimize the surface of the SLM. The property of declaring a spatial, shape-wise restriction on the Gerchberg-Saxton Algorithm is used as the primary optimization factor that enables us to classify various objects based on the shape-based characteristics of the object.

## **Noise Addition Process and Testing**

To test the performance of our method, a synthetic, randomly-noise-induced datasets with various level of noise have been created. The noise adding process, depicted as in Supp. Fig 1A, flips the values of the binary image either constructively [ $0 \rightarrow 1$ ] or destructively [ $1 \rightarrow 0$ ]. The position of the noisy pixels were selected randomly and selected once. With this rule, double selection (i.e.  $0 \rightarrow 1 \rightarrow 0$ ) is prevented. To test each noise induced image, it is grid wise multiplied to cover the whole sub-surfaces available on the SLM. This grid wise multiplication is depicted on Supp. Fig 1B. The final binary mask is then element wise multiplied with the final trained phase mask and tested on the SLM.



## References

- [1] János Véghe. “How Amdahl’s Law limits the performance of large artificial neural networks”. In: *Brain Informatics* 6.1 (Apr. 11, 2019). DOI: 10.1186/s40708-019-0097-2. URL: <https://doi.org/10.1186/s40708-019-0097-2>.
- [2] Radosvet Desislavov, Fernando Martínez-Plumed, and José Hernández-Orallo. “Trends in AI inference energy consumption: Beyond the performance-vs-parameter laws of deep learning”. In: *Sustainable Computing Informatics and Systems* 38 (Feb. 26, 2023), p. 100857. DOI: 10.1016/j.suscom.2023.100857. URL: <https://doi.org/10.1016/j.suscom.2023.100857>.
- [3] Joseph W. Goodman. *Introduction to Fourier Optics*. Roberts and Company Publishers, Jan. 1, 2005.
- [4] H.J. Caulfield, J. Kinser, and S.K. Rogers. “Optical neural networks”. In: *Proceedings of the IEEE* 77.10 (Jan. 1, 1989), pp. 1573–1583. DOI: 10.1109/5.40669. URL: <https://doi.org/10.1109/5.40669>.
- [5] Francis T.S. Yu. *II Optical Neural Networks: architecture, design and models*. Jan. 1, 1993, pp. 61–144. DOI: 10.1016/s0079-6638(08)70162-8. URL: [https://doi.org/10.1016/s0079-6638\(08\)70162-8](https://doi.org/10.1016/s0079-6638(08)70162-8).
- [6] Ying Zuo et al. “Scalability of All-Optical neural networks based on spatial light modulators”. In: *Physical Review Applied* 15.5 (May 17, 2021). DOI: 10.1103/physrevapplied.15.054034. URL: <https://doi.org/10.1103/physrevapplied.15.054034>.
- [7] Li Deng. “The MNIST Database of Handwritten Digit Images for Machine Learning Research [Best of the Web]”. In: *IEEE Signal Processing Magazine* 29.6 (Oct. 19, 2012), pp. 141–142. DOI: 10.1109/msp.2012.2211477. URL: <https://doi.org/10.1109/msp.2012.2211477>.
- [8] Han Xiao, Kashif Rasul, and Roland Vollgraf. “Fashion-MNIST: a Novel Image Dataset for Benchmarking Machine Learning Algorithms”. In: *arXiv (Cornell University)* (Jan. 1, 2017). DOI: 10.48550/arxiv.1708.07747. URL: <https://arxiv.org/abs/1708.07747>.
- [9] Tiankuang Zhou et al. “Large-scale neuromorphic optoelectronic computing with a reconfigurable diffractive processing unit”. In: *Nature Photonics* 15.5 (Apr. 12, 2021), pp. 367–373. DOI: 10.1038/s41566-021-00796-w. URL: <https://doi.org/10.1038/s41566-021-00796-w>.
- [10] Xing Lin et al. “All-optical machine learning using diffractive deep neural networks”. In: *Science* 361.6406 (July 26, 2018), pp. 1004–1008. DOI: 10.1126/science.aat8084. URL: <https://doi.org/10.1126/science.aat8084>.

- [11] Che Liu et al. “A programmable diffractive deep neural network based on a digital-coding metasurface array”. In: *Nature Electronics* 5.2 (Feb. 21, 2022), pp. 113–122. DOI: 10.1038/s41928-022-00719-9. URL: <https://doi.org/10.1038/s41928-022-00719-9>.
- [12] J. D. Paola and R. Schowengerdt. *The effect of Neural-Network structure on a multispectral Land-Use/Land-Cover classification*. 1997. URL: <https://api.semanticscholar.org/CorpusID:130948625>.
- [13] Gerchberg R. W. “A practical algorithm for the determination of phase from image and diffraction plane pictures”. In: *CiNii Research* (1972). URL: <http://ci.nii.ac.jp/naid/10025518647/>.
- [14] Ting-Chung Poon and Jung-Ping Liu. *Introduction to modern digital holography*. Jan. 5, 2014. DOI: 10.1017/cbo9781139061346. URL: <https://doi.org/10.1017/cbo9781139061346>.
- [15] Da Costa Gabriel B. Paranhos et al. *An empirical study on the effects of different types of noise in image classification tasks*. Sept. 9, 2016. URL: <http://arxiv.org/abs/1609.02781>.
- [16] Samuel Dodge and Lina Karam. “Understanding how image quality affects deep neural networks”. In: June 1, 2016, pp. 1–6. DOI: 10.1109/qomex.2016.7498955. URL: <https://doi.org/10.1109/qomex.2016.7498955>.
- [17] Nabendu Chaki, Soharab Hossain Shaikh, and Khalid Saeed. *A comprehensive survey on image binarization techniques*. Jan. 1, 2014, pp. 5–15. DOI: 10.1007/978-81-322-1907-1\_2. URL: [https://doi.org/10.1007/978-81-322-1907-1\\_2](https://doi.org/10.1007/978-81-322-1907-1_2).
- [18] Reddy. *API design for C++*. Jan. 1, 2011. DOI: 10.1016/c2010-0-65832-9. URL: <https://doi.org/10.1016/c2010-0-65832-9>.
- [19] Randal E. Bryant and David R. O’Hallaron. *Computer Systems: A Programmer’s Perspective, Global Edition*. Pearson Higher Ed, July 12, 2019.
- [20] Jürgen Schmidhuber. “Deep learning in neural networks: An overview”. In: *Neural Networks* 61 (Oct. 13, 2014), pp. 85–117. DOI: 10.1016/j.neunet.2014.09.003. URL: <https://doi.org/10.1016/j.neunet.2014.09.003>.

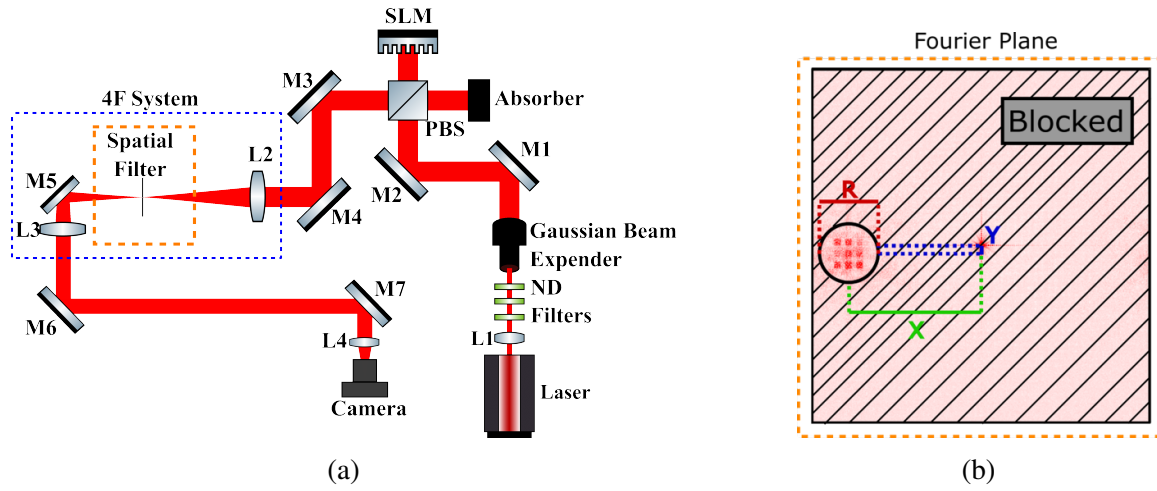


Figure 1: **A**, The schematic illustration of the optical system. **B**, The Fourier Plane at the Spatial Filter. Only a circular region at the position  $(X, Y)$  with a diameter of  $R$  is passed through by the Spatial Filter. L: Lens, M: Mirror, ND: Neutral Density, PBS: Polarizing Beam Splitter, SLM: Spatial Light Modulator.

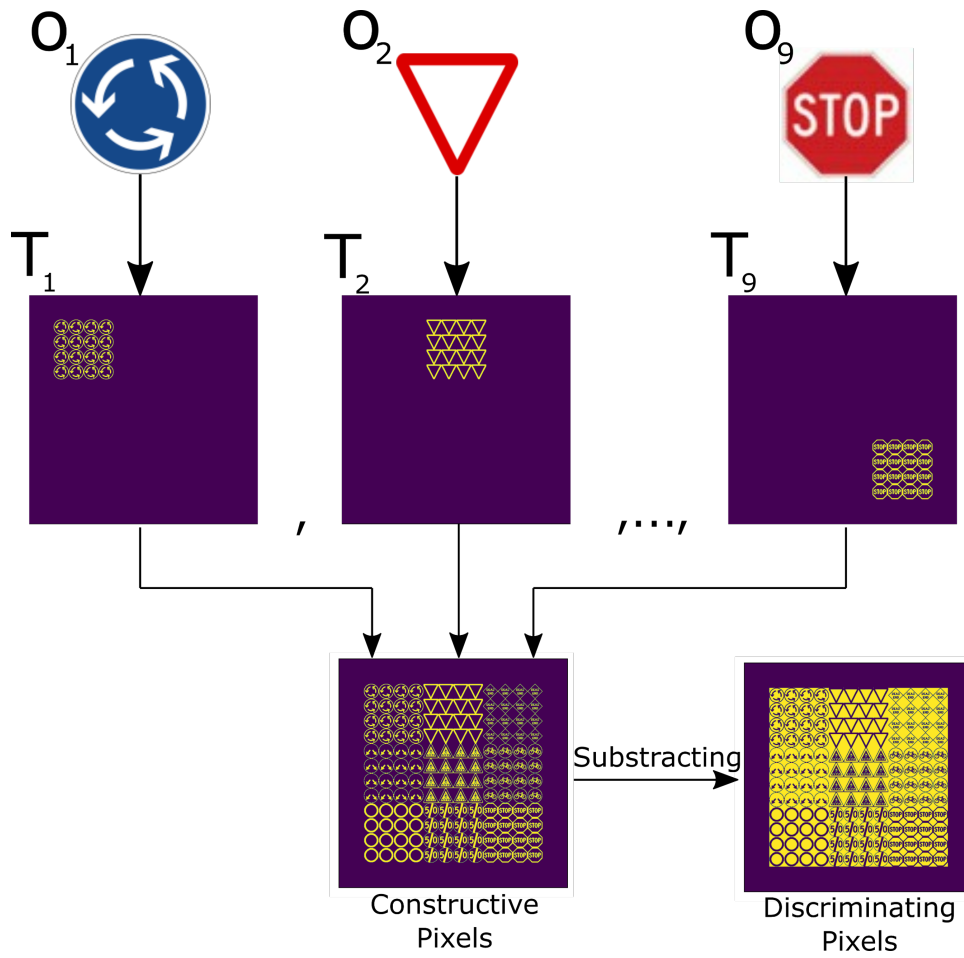


Figure 2: The grid-wise multiples of the object's binary image is placed into the corresponding sub-surface. The excluding pixels are used to diverge the light outside the target areas.

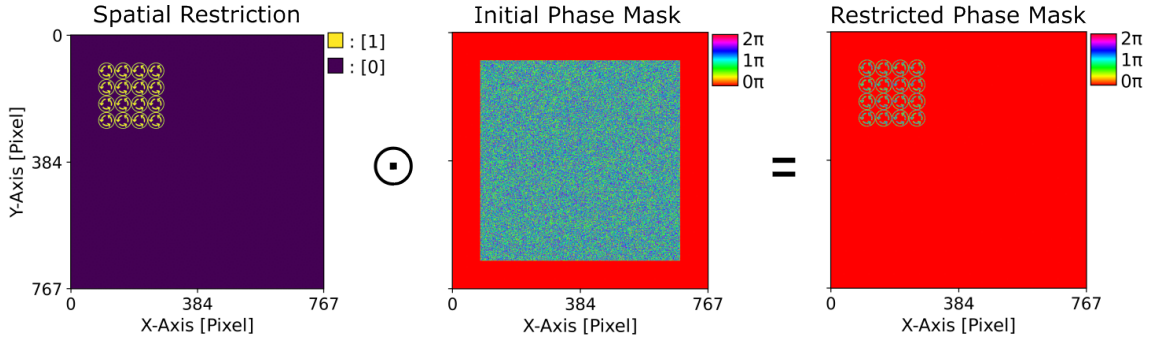


Figure 3: The binary form of the Spatial Restriction Array is used in element-wise multiplication to include only the Constructive Pixels of the object which is optimized via the Gerchberg-Saxton Algorithm.

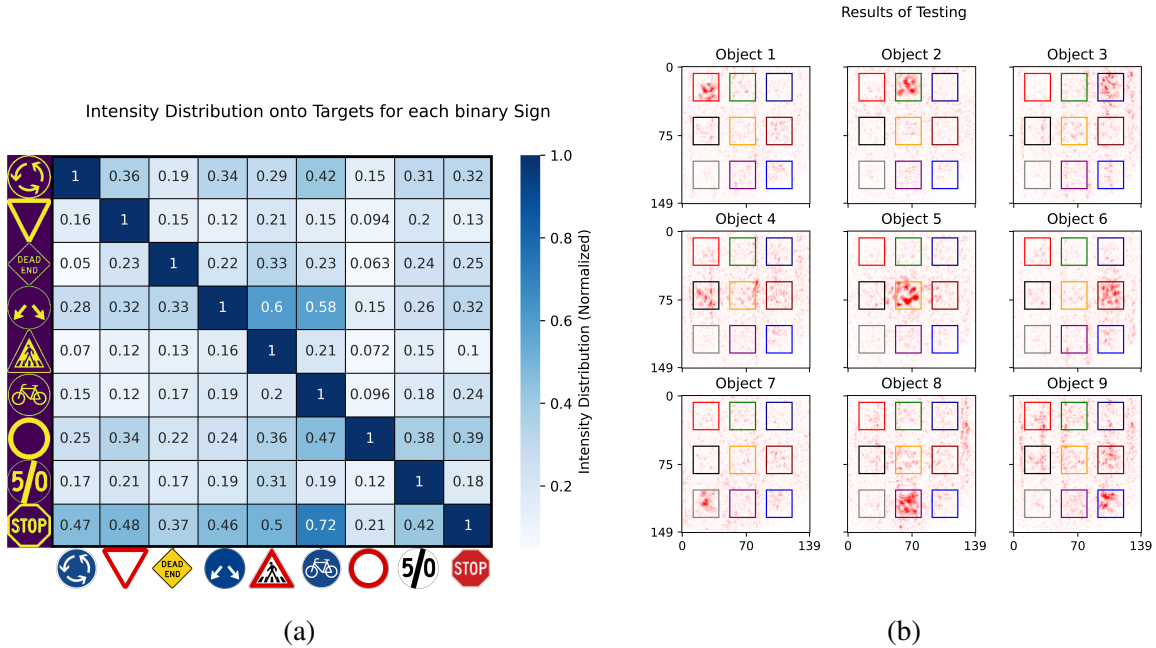
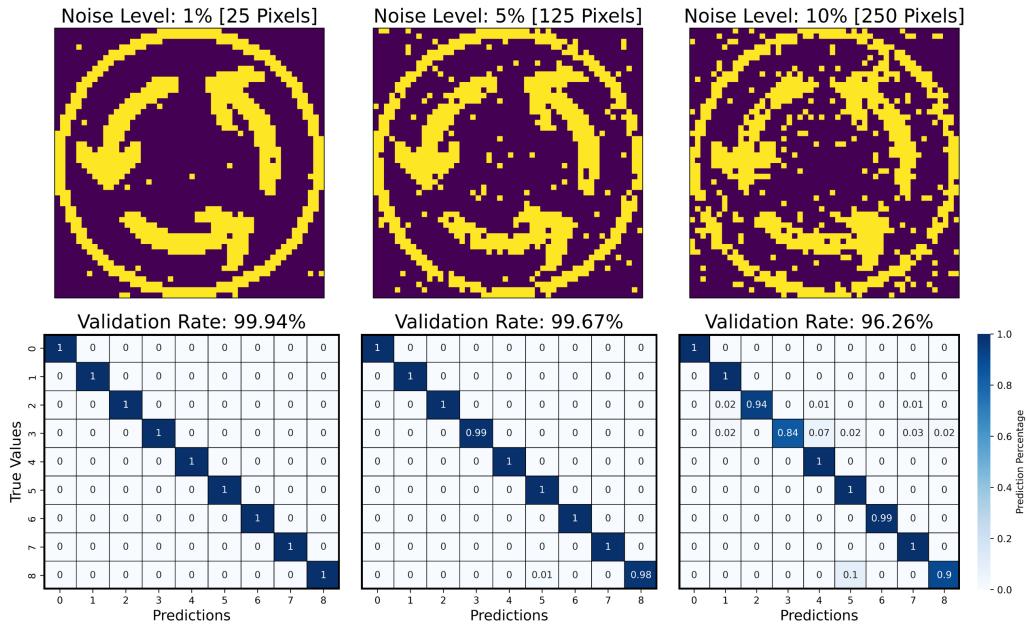
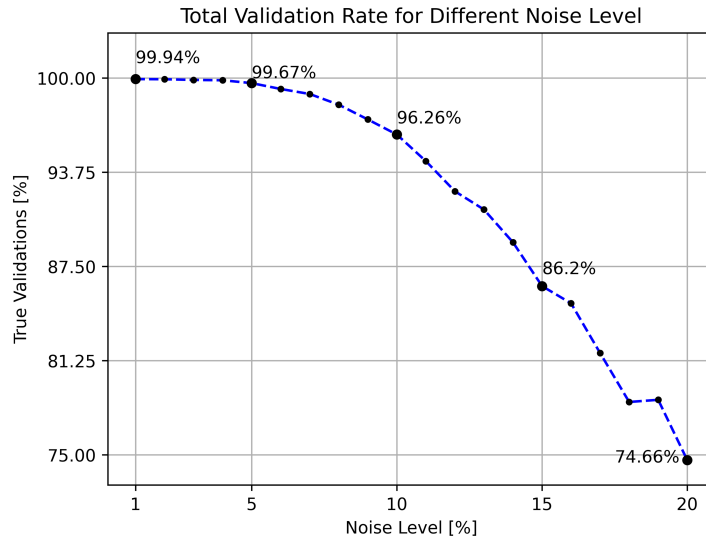


Figure 4: **A**, The generated phase plate is tested for the power distribution performance. The binary and grided form of the traffic signs were used to obtain the result. The intensity distribution is showed as a matrix form were each row corresponds to the histographic intensity distribution were the values are normalized according to the maximum value. **B**, The targets used in the optimization process are 3x3 grid with constant height, width, horizontal and vertical separation. The coordinate system of the Fourier Plane in the algorithm and the coordinate system of the real Fourier Plane on the camera are not mapped exactly since the magnification provided by the 4F system and slight misalignment. Therefore, there is a slight linear transformation between those Fourier Planes. On the figure, the Intensity Distribution is shown when a object is placed on the SLM.

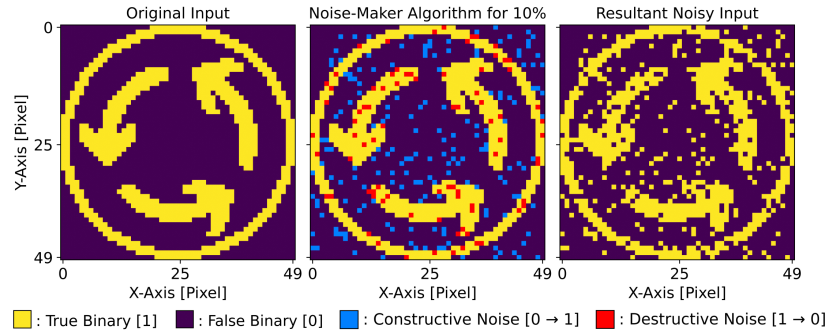


(a)

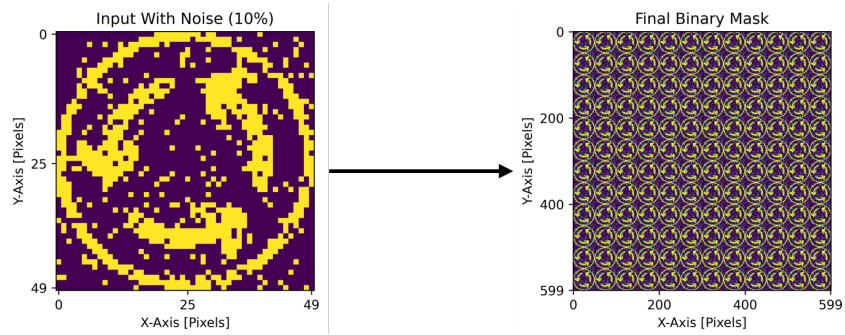


(b)

Figure 5: **A**, The noisy validation images are generated with the same algorithm shown in Figure 4 was used to generate a dataset of 9000 images (1000 for each object) for every noise percentages. The test results for 1%, 5% and 10% are shown with a sample from the noisy dataset and their corresponding Confusion Matrices. With 10% noise, a validation rate of 96.26% was archived. **B**, The results of each validation test for the range [1%, 20%] with 1% is shown as a line plot where also the results of {1%, 5%, 10%, 15%, 20%} is annotated with their results. With a noise percentage of 20%, the algorithm has successfully labeled 74.66% of the images.



(a)



(b)

Supplementary Figure 1: **A**, A random noise that modifies the image in either Constructive [0 → 1] or Destructive [1 → 0] was applied. The percentage (or the amounts of pixels) varies for each test from 1% to 20% with 1% steps. The Constructive and Destructive noise was shown with blue and red pixels respectively. **B**, The input with noise is grid wise multiplied with the same grid size as the trained phase mask. The result from element wise multiplication of the final binary mask and the optimized phase mask is then inserted to the SLM to test each noise degree on each image.